Journal of Quantitative Spectroscopy & Radiative Transfer 255 (2020) 107225

Contents lists available at ScienceDirect

Journal of Quantitative Spectroscopy & Radiative Transfer

journal homepage: www.elsevier.com/locate/jqsrt

A new model of monodeuterated ethane (C_2H_5D) spectrum: Enabling sensitive constraints on the D/H in ethane emission in comets

Kirstin D. Doney[a,*], Vincent Kofman[c,d], Geronimo Villanueva[c], Keeyoon Sung[b]

[a] National Institute of Standards and Technology, JILA, Boulder, CO 80309, USA
[b] Jet Propulsion Laboratory, California Institute of Technology, Pasadena, CA 91109, USA
[c] NASA - Goddard Space Flight Center, Planetary Systems Laboratory (693), Greenbelt, MD 20771, USA
[d] American University, Washington, DC 20016, USA

ARTICLE INFO

Article history:
Received 3 April 2020
Revised 24 June 2020
Accepted 19 July 2020
Available online 20 July 2020

Keywords:
Infrared
Rovibrational spectra
Comets
Deuterium fractionation

ABSTRACT

Similar to ethane (C_2H_6), monodeuterated ethane (C_2H_5D) has a bright series of Q-branches in the CH stretch region, between about 2960 - 3020 cm^{-1} (3.38 - 3.31 μm). As the progressions in the different isotopes are slightly offset from one another, the new C_2H_5D model enables sensitive constrains of the D/H ratio in spectra from comets, in organics across the Solar System and beyond. Specifically, the D/H ratio of organic molecules in comets is a critical cosmogenic indicator, which not only provides insights into the formation processes of our Solar System, but also allows for a test of our understanding of solid-state astrochemistry. High D/H ratios are predicted in a number of astrochemical models, which can be benchmarked using the new spectroscopic information of C_2H_5D and C_2H_6. We present a quantum band model for C_2H_5D in the mid-infrared. Our model is based on rotationally resolved spectra of C_2H_5D and C_2H_6 obtained at 85K between 2050 - 3050 cm^{-1} (4.88 - 3.28 μm) using a Bruker IFS-125HR equipped with a cryogenic Herriott cell at JPL. High-level quantum chemical calculations were carried out at the CCSD(T)/ANO1 level of theory to aid vibrational assignments, with the anharmonic frequencies and vibrational corrections determined from second-order vibrational perturbation theory (VPT2). As a first demonstration of the applicability of the model, we obtained a stringent upper limit to the organic D/H ratio (18.2 VSMOW) in comet C/2007 W1 (Boattini) from high resolution fluorescence spectra obtained with Keck/NIRSPEC.

Published by Elsevier Ltd.

1. Introduction

One of the outstanding astronomical questions of modern times is understanding the chemical evolution of our planetary system; of particular interest is the origins of the chemical composition of Earth. Since all deuterium (D, heavy hydrogen) was formed during the Big Bang, and subsequently been depleted through astration or integration in molecules [1,2], the isotopic ratio of deuterium to hydrogen (D/H) is a valuable measure of the chemical history of astronomical objects. In the solar system, the D/H ratio on Earth (determined from H_2O) differs widely from that known for other planets in our solar system, but is consistent with the values observed for Oort cloud and Jupiter family comets suggesting comets are the source for deuterium enrichment [3–5]. While, the protosolar D/H value is approximately preserved in the giant planets, at a value roughly 2×10^{-5} [6,7], the rocky planets show about an order of magnitude greater deuterium enrichment, likely as a result of atmospheric water loss [8,9].

Deuterium enrichment occurs through a number of mechanisms, most of which are driven by the small difference in the zero point energy between hydrogen and deuterium. Consequently, isotopic fractionation is sensitive to formation conditions and temperatures. In the gas-phase, it occurs through, e.g., photodestruction of HD to D and ion-neutral reactions with H_2D^+ [10–12]. Low temperatures, such as those found in cold molecular clouds in the interstellar medium (ISM) or midplane of protoplanetary disks (< 50 K), result in strong deuterium enrichment because kinetic energies favor dehydrogenation over dedeuteration. Moreover, in these regions of space, molecules freeze out of the gas phase, and grain-surface chemistry is thought to further enhance the D/H ratio of interstellar ice species, leading to a significantly deuterium enriched ice layer ([13,14] and references therein).

Comets are formed in the “freeze-out zone” of protoplanetary disks of forming solar systems, and consequently they act as cryogenic relics of the original molecular cloud [15]. Through

* Corresponding author.
E-mail address: Kirstin.Doney@nist.gov (K.D. Doney).

https://doi.org/10.1016/j.jqsrt.2020.107225
0022-4073/Published by Elsevier Ltd.

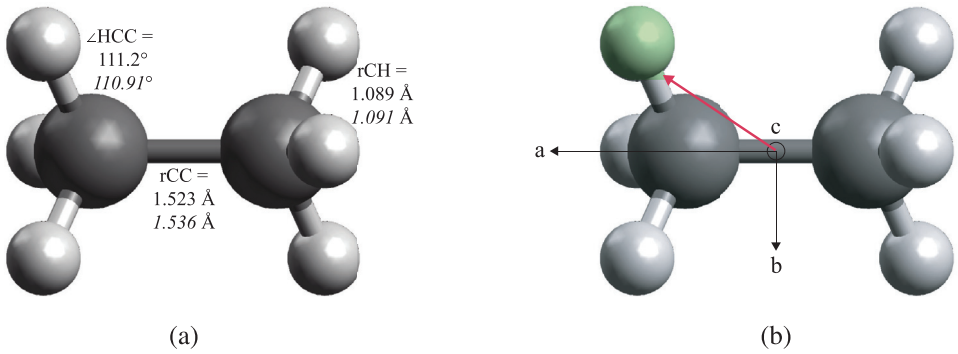

Fig. 1. The CCSD(T)/cc-pCVQZ geometry of a) C_2H_6 and b) C_2H_5D; the rotational axes are shown in panel b) apply to both molecules. The a-axis, which has the smallest moment of inertia, lies along the C-C bond, while the c-axis, which has the largest moment of inertia, is directed into the page. The *ab initio* bond lengths and angle are given for C_2H_6, with experimentally determined values givin in italics below [30]. The permanent dipole moment (red arrow) of C_2H_5D is in the a/b-plane, with a magnitude of $\sim$0.0078 D.

understanding the chemical composition of comets we can test the hypothesis that small icy bodies delivered prebiotic matter to early Earth. To date the D/H ratio in comets is known primarily from measurements of H_2O, and limited measurements of HCN and CH_4 ([16–22] and references therein). Strong differences in the D/H ratios are expected between water and carbon bearing molecules, with hydrocarbons expected to show high deuterium enrichments (see the model described in Cleeves et al. [23]). For example in the ISM, high D/H ratios ($\sim$0.2) are seen, e.g., for CH_3OH, polycyclic aromatic hydrocarbons (PAHs), and NH_3 [14,24–26].

Ethane (C_2H_6) offers a good probe of cometary D/H ratio as it is often one of the molecules that dominates the mid-infrared (mid-IR) spectra (3 - 5 µm) of the comae [27,28]. Of the deuterated isotopologues, monodeuterated ethane (C_2H_5D) is statistically expected to be the most likely form. Importantly, the monodeuterated isotopologue has strong features near both 3.4 µm and 4.6 µm. This give the advantage of simultaneous measurement of features for C_2H_6 and C_2H_5D, reducing systematic errors in determining D/H ratios.

Cometary C_2H_6 was first detected in the comet C/1996 B2 (Hyakutake) through observation of the CH_3 asymmetric stretch (ν_7) fundamental band emission features around 3.35 µm [27]. Since its first identification, and considering that the infrared C_2H_6 signatures are so strong, it is now considered a primary tracer to the volatile composition of cometary ices. The abundance of C_2H_6 is found to be on order of a few tenths of a percent with respect to water, similar to methane abundances [29]. However, in order to measure the D/H ratio using ethane, accurate rovibrational data for both isotopologues is needed.

The equilibrium geometry of $C_2H_6(\tilde{x}^1A_{1g})$ consists of two methyl groups that are staggered with respect to each other (see Fig. 1a). As such, it is a centrosymmetric molecule with no permanent dipole moment, and cannot be detected through its pure rotational transitions. Instead its detection is through the infrared active vibrational modes, which have been well studied in the laboratory, including all fundamental and some combination bands [28,31–39]. Of the infrared active modes, remote sensing is often carried out through the strongest band - the ν_7 fundamental band at $\sim$2985 cm^{-1}. Recently, Villanueva et al. [28] extensively modelled the C_2H_6 rovibrational spectra around the ν_7 band, describing over 17,000 transitions in this region, including transitions of a nearby hot-band.

Deuterium atoms can replace hydrogen atoms in molecules, and participate in the same characteristic vibrations. The substitution of one hydrogen atom with a deuterium atom results in monodeuterated ethane (C_2H_5D; $\tilde{x}^1A'$), which has a permanent dipole moment ($\sim$0.0078 D; see Fig. 1b). Accordingly, pure rotational transitions are now allowed, and all eighteen vibrational modes are infrared active. C_2H_5D is comparatively less well spectroscopically studied, with only the lowest three rovibrational manifolds (ground, ν_{18}, and ν_{17}) being known [40,41]. Precise spectroscopic data comes from the study by Daly et al. [40], combining room temperature submillimeter data between 8.7 and 53 cm^{-1} (between 260 and 1600 GHz) with microwave data from Hirota et al. [42] to determine ground and torsionally excited state parameters for C_2H_5D, including the sextic centrifugal distortion rotational constants and fourth order tunneling terms. However, for the majority of the studied rovibrational manifolds only the approximate vibrational energy is experimentally known, if at all; this includes all of the CD and CH stretch vibrational modes [43,44].

In this work, we present the high resolution infrared spectra of C_2H_6 and C_2H_5D in the mid-IR, and the application of the rovibrational models to derive a sensitive upper-limit of D/H ratio in comets. This article is organized as follows. Section 2 contains details of the experimental methods for measuring the gas-phase infrared spectra of C_2H_6 and C_2H_5D. Section 3 discusses the spectral analysis and vibrational assignments, including the results of high level *ab initio* calculations. In the C_2H_5D model, we present a complete quantum mechanical band model for eight bands, including lines of P, Q, and R branches. The modelled spectrum is applied to a fluorescence model, and the astrophysical implications are discussed in Section 4. Finally, in Sections 5 the conclusions are presented.

2. Experimental method

The experimental setup has been described in detail in Sung et al. [45] and Mantz et al. [46]. In the present experiment, the molecules under study are obtained from ICON at high purity and used as is: 99.99% ethane (C_2H_6) and 98% 1D-enriched ethane (C_2H_5D). The gas is injected into a cryogenically cooled gas cell kept at $\sim$85 K, and a pressure of about 0.293 Pa; at such low pressures there is uncertainty in the pressure reading

The IR spectrum of gas-phased molecules is recorded using a high resolution Fourier transform spectrometer, Bruker IFS-125HR, at JPL, wherein the IR beam is multipassed with Herriott cell optics resulting in an absorbance path length of 20.941 m. The final transmission spectra are recorded as a function of frequency over 22 and 50 hours for C_2H_6 and C_2H_5D, respectively. The resulting resolution of the spectra is 0.0019 cm^{-1}, which is approximately

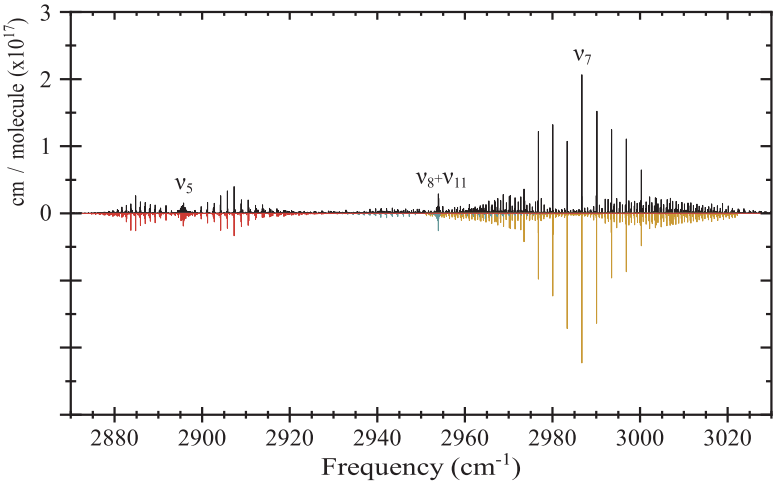

Fig. 2. The experimental gas-phase spectra of C_2H_6 at 85 K between 2870 - 3030 cm^{-1} (3.48 - 3.30 μm, in black), with the inverted simulated rovibrational bands plotted below in color (using the PGOPHER software [47]). The vibrational assignments are given above the corresponding band origin.

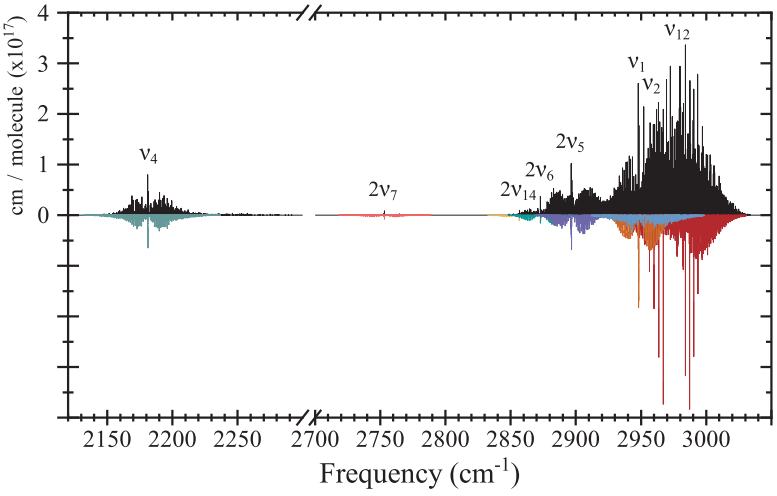

Fig. 3. The experimental gas-phase spectra of C_2H_5D at 85 K between 2150 - 3050 cm^{-1} (4.65 - 3.28 μm, in black), with the inverted simulated rovibrational bands plotted below in color (using the PGOPHER software [47]). The vibrational assignments are given above the corresponding band origin.

the Doppler broadened line-width at the given frequency. The absolute frequencies are obtained by calibration against CO_2.

3. Monodeuterated ethane model

The infrared spectra of C_2H_6 and C_2H_5D are recorded between 2050 - 3050 cm^{-1} (4.88 - 3.28 μm). The experimental transmission signal (I) is converted to absorption cross sections (σ, in cm/molecule) from the expression:

$$\sigma = \frac{-ln(I)}{NL} \quad (1)$$

where L is the path length and N is the species concentration. The recorded overview spectra are shown in Figs. 2 and 3. Three rovibrational bands of C_2H_6 and eight rovibrational bands of C_2H_5D are observed.

Previous experimental and theoretical work showed that this region is dominated by the CH and CD stretch vibrations [28,31,43,48,49]. C_2H_6 is a prolate symmetric top molecule, and the infrared active rovibrational bands can be broken up into two structure type: parallel bands of A_u symmetry, which are identified by close spacing of the *K*-subband Q-branches, and perpendicular bands of E_u symmetry, which is identified by significantly larger spacing between the *K*-subband Q-branches. In contrast, as a near-prolate asymmetric top molecule of C_s symmetry, the rovibrational band structure for C_2H_5D is relatively more complex with three types of band structure that depends on the direction of the transition dipole moment: A-type, which is identified by close spacing of K_a-subband Q-branches, and B- and C-type, which are identified by larger spacing between the K_a-subband Q-branches. Furthermore, since the D-atom lies in the a-/b-axis plane, but not along either axis, the permanent dipole moment points in the direction of the D-atom between the a- and b-axis. As a result the rovibrational bands of C_2H_5D exhibit a band structure composed of either purely C-type transitions or a mixture of A- and B-type transition. The relative intensity of the A- and B-type transitions depends on the magnitude of the transitional dipole moments (μ), *i.e.*, a larger μ_A relative to μ_B results in a rovibrational band structure composed of strong A-type transitions with accompanying weaker B-type transitions.

At the spectral resolution of the present rotationally cold gas-phase spectra, the individual rovibrational transitions are resolvable, allowing for rotational analysis and unambiguous vibrational assignment. Based on the experimental conditions, a gas temperature of 85 K, vibrational transitions out of the ground vibrational state are dominant from Boltzmann statistics. The rotational analysis of the ethane bands is performed using the PGOPHER software

[47] starting from a symmetric top Hamiltonian, while the rotational analysis of C_2H_5D bands is performed starting from a Watson non-rigid asymmetric top Hamiltonian (A reduction and Ir representation). In all fits, the ground state rotational constants are fixed to the values given by Pine and Lafferty [33] and Daly et al. [41] for C_2H_6 and C_2H_5D, respectively. The band profiles and relative band intensities are consistent with a molecular rotational temperature of ~85 K. In the initial fits, individual rotational transitions are identified, up to $J'' = 15$, $K_a'' = 15$, and $K_c'' = 15$.

To accurately model the rovibrational bands of both C_2H_6 and C_2H_5D, torsional (internal rotation) terms should be included in the Hamiltonian, which acts as a small perturbation to the rovibrational energy levels, and subsequently, the transition line positions. However, these terms could not be included accurately in the PGOPHER model [47]. For the purpose of this study, the experimental spectrum is convoluted with a Gaussian function to closer mimic the expected resolution of astronomical spectra ($\Delta\nu$ = 0.05 cm^{-1}), and performed a contour fit of the rovibrational band profile to refine the rotational analysis. Using this method, ideally the small line positions shifts expected from the torsion could be neglected. Fortunately, the effect of the internal torsional motion of the D-atom around the molecular symmetry axis relative to the CH_3 group in C_2H_5D and the effect of the CH_3 groups relative to each other in ethane is observed to be minor. At the smoothed resolution the standard rovibrational Hamiltonians are able to reproduce the observed band profiles, allowing for determination of effective spectroscopic parameters.

The upper state vibrational assignments are made based on the vibrational energies, ν_0, and the primary rotational constants (A_v, B_v, and C_v). For new vibrational states, the vibrationally dependent rotational constants are estimated, to first order approximation, from:

$$X_v = X_0 - \sum_i (\alpha_i^X v_i) \tag{2}$$

where X is used as a generalization for A, B, and C, A_0, B_0, and C_0 are the experimentally determined ground state values [28,41], α_i^X are the VPT2 vibration-rotation interaction constants determined from *ab initio* calculations, and v_i is the vibrational quantum number.

Spectral analyses of the bands are performed by fixing the ground state rotational constants to the previously determined values, and fitting the observed transitions using least-squares analysis to determine the band origin, and effective upper state rotational constants (A′, B′, and C′). The resulting vibrational assignments and spectroscopic parameters are summarized in Tables 3 and 4. In addition to the expected CH and CD fundamental bands, one combination band and four overtone bands out of the ground state are assigned for C_2H_6 and C_2H_5D, respectively.

By varying the modelled transition dipole moments to match simulated line intensities to the observed line intensities the spontaneous Einstein A coefficients were determined from the expression:

$$A_{AB} = \frac{8\pi^2 \nu_{AB}^3}{3\varepsilon_0 c^3 \hbar} |\langle A|\mu|B\rangle|^2 \tag{3}$$

which can be approximated to:

$$A_{AB} = (3.13618894 \times 10^{-7} s^{-1} cm^{-3} Debye^{-2}) \nu_{AB}^3 S \tag{4}$$

where ν_{AB} is the transition frequency between states A and B, and S is the line strength. The determined Einstein A values and line positions are used as the input for the fluorescence model.

3.1. Ab initio calculations

To support the vibrational assignment of the observed rovibrational bands, high level quantum chemical calculations were performed with the development version of the CFOUR program [50]. The computational method is calibrated using the frequencies of the well studied C_2H_6 and rotational constants of known C_2H_5D states.

All calculations were carried out at the CCSD(T) level of theory, which with a sufficiently large basis set has been shown to accurately reproduce experimental values of semi-rigid molecules [51–61]. Equilibrium geometries were determined using the large core-valence correlation-consistent quadruple-ζ basis set (cc-pCVQZ), which features [8s7p5d3f1g] (non-hydrogen atoms) and [4s3p2d1f] (hydrogen) of (15s9p5d3f1g) and (6s3p2d1f) primitive basis sets, respectively [62–64]. All electron (AE)-CCSD(T)/cc-pCVQZ has been shown to give accurate equilibrium geometries for small hydrocarbons [58,60,61,65–67].

It is well known that correlation-consistent basis sets, such as cc-pCVQZ, are susceptible to basis set superposition error (BSSE) [68,69]. One way to avoid this possible problem is to use basis sets with a large number of Gaussian primitives (particularly f-type), such as the atomic natural orbital (ANO) basis set (with the primitive basis set (13s8p6d4f2g) for non-hydrogen atoms and (8s6p4d2f) for hydrogen) [56,70,71]; the basis set has common truncations: [4s3p2d1f] for non-hydrogen atoms and [4s2p1d] for hydrogen (hereafter known as ANO1) [63,64,70]. In addition, only the valence electrons of carbon are considered in the correlation treatment, *i.e.*, standard frozen-core (fc) calculations. (fc)-CCSD(T)/ANO1 has been shown to accurately reproduce experimental frequencies and intensities for small molecules [56,60,61,72,73]. Using the (fc)-CCSD(T)/ANO1 optimized geometry, second-order vibrational perturbation (VPT2) theory calculations were determined from full cubic and the semidiagonal part of the quartic force fields obtained by numerical differentiation of analytic CCSD(T) second derivatives [54,74]. Due to the high density of states in the 3 µm region, particularly for C_2H_5D, in order to reproduce the observed vibrational frequencies resonances between states must be addressed. The vibrational frequencies resulting from the resonant interactions are calculated by a deperturbation-diagonalization technique followed by transformation of the deperturbed transition moments, as discussed in Vázquez et al. [73] and Matthews et al. [74].

The CCSD(T)/cc-pCVQZ equilibrium geometries (see Fig. 1) of C_2H_6 and C_2H_5D result in equilibrium rotational constants of A_e = 2.7041 and B_e = 0.6711 cm^{-1} for C_2H_6, and A_e = 2.3511, B_e = 0.6365, and C_e = 0.6147 cm^{-1} for C_2H_5D. The VPT2 vibrational corrections to the equilibrium rotational constants result in ground state rotational constants of A_0 = 2.6687 and B_0 = 0.6622 cm^{-1} for C_2H_6, which agree within ~0.1% of the experimental values of 2.671 and 0.6630271 cm^{-1}, respectively [33]. Similarly, for C_2H_5D, the ground state rotational constants, A_0 = 2.3225, B_0 = 0.6283, and C_0 = 0.6068 cm^{-1}, agree with the reported experimental values of 2.323387, 0.629071, and 0.607559 cm^{-1}, respectively [40].

3.2. Rovibrational structure of C_2H_6

The experimental spectra of this region (see Fig. 2), agrees with previous studies from Pine and Lafferty [33] and Hepp and Herman [37], and shows only three strong rovibrational bands with band origins at: 2895.62(1) cm^{-1} (A_{2u}), 2953.92(2) cm^{-1} (A_{2u}), and 2985.39(1) cm^{-1} (E_u), and a weak band at 2930 cm^{-1} (E_u). Comparison of current determined band origins with previous experimental studies assign these bands as the $\nu_8 + \nu_{11}$ combination band, the ν_5 fundamental band, and the ν_7 fundamental band (see Table 3) [28,33,37].

The CCSD(T)/ANO1 VPT2 calculations are consistent with the experimental observations. As a highly symmetric molecule C_2H_6 is predicted to have only three strong infrared active modes in the 3 µm region: $\nu_8 + \nu_{11}$ ($A_{1u} \oplus A_{2u} \oplus E_u$), ν_5 (A_{2u}), and ν_7 (E_u),

Table 1
Harmonic (ω) and anharmonic (VPT2, ν) frequencies (in cm^{-1}) of fundamental and select combination states C_2H_6 and C_2H_5D[a].

Mode	CCSD(T)/ANO1		Expt.	Expt.-Calc.
	ω	ν	ν	
C_2H_6				
ν_1 (A_{1g})	3040.4	2981.3	2953.7[a]	-27.6
ν_2 (A_{1g})	1424.4	1393.3	1388.4[a]	-4.9
ν_3 (A_{1g})	1011.9	988.4	993.959(94)[b]	5.5
ν_4 (torsion)	313.0	294.8	289.52[c]	-5.3
ν_5 (A_{2u})	3039.9	2984.1	2895.62(1)[d]	-88.5
ν_6 (A_{2u})	1406.2	1375.4	1379.163(4)[f]	3.7
ν_7 (E_u)	3124.3	2984	2985.39(1)[d]	1.4
ν_8 (E_u)	1509.8	1468.8	1471.634(9)[f]	2.5
ν_9 (E_u)	820.5	818.4	821.72244[g]	3.3
ν_{10} (E_g)	3101.4	2959.7	2968.48(10)[h]	8.8
ν_{11} (E_g)	1508.8	1465.6	1468.4(1)[h]	2.8
ν_{12} (E_g)	1225.0	1195.6	1196.9(2)[h]	1.3
$\nu_4 + \nu_{12}$ (E_u)	1538.1	1484.8	1479.807(9)[f]	-5.3
$2\nu_4 + \nu_8$ (E_g)	2135.9	2029.3	2014.08(30)[h]	-15.2
$\nu_{11} + \nu_{12}$ (E_g)	2733.9	2657.8	2658.29(5)[h]	0.5
$\nu_8 + \nu_{12}$ (A_{2u})	2734.9	2659.7	2665.1512(30)[i]	5.5
$\nu_2 + \nu_6$ (A_{2u})	2830.6	2749.9	2753.326(32)[i]	3.4
$\nu_6 + \nu_{11}$ (E_u)	2915.1	2838.6	2844.13069(75)[i]	5.5
$\nu_8 + \nu_{11}$ (A_{2u})	3018.7	2894.0	2953.92(2)[d]	59.9
$\nu_8 + \nu_{11}$ (E_u)	3018.7	2931.8	2930.705(90)[i]	-1.1
$\nu_4 + \nu_{10}$ (E_u)	3414.4	3255.5	3255.568(50)[i]	0.1
$\nu_4 + \nu_7$ (E_g)	3437.3	3275.6	3256.55(4)[h]	-19.0
ZPE = 16173.8 cm^{-1}				
C_2H_5D				
ν_1 (A')	3114.0	2951.4	2948.30(1)[d]	-3.1
ν_2 (A')	3065.5	2956.9	2952.18(5)[d]	-4.7
ν_3 (A')	3040.2	2980.8		
ν_4 (A')	2263.8	2177.3	2181.38(1)[d]	4.1
ν_5 (A')	1509.0	1468.6	1469[j]	0.4
ν_6 (A')	1485.2	1452.4	1449[j]	-3.4
ν_7 (A')	1415.9	1384.8	1388[j]	3.2
ν_8 (A')	1326.5	1296.6	1310[j]	13.4
ν_9 (A')	1143.4	1119.4	1120[j]	0.6
ν_{10} (A')	994.2	973.2	978[j]	4.8
ν_{11} (A')	714.4	712.4	711[k]	-1.4
ν_{12} (A")	3124.2	2977.9	2975.71(1)[d]	-2.2
ν_{13} (A")	3101.2	2956.3		
ν_{14} (A")	1509.3	1443.1		
ν_{15} (A")	1340.5	1307.6	1312[j]	4.4
ν_{16} (A")	1186.9	1158.3	1159[j]	0.7
ν_{17} (A")	805.0	802.0	805.342729(27)[l]	3.3
ν_{18} (torsion)	293.7	277.2	271.1[k]	-6.1
$2\nu_9$ (A')	2286.8	2239.0		
$2\nu_7$ (A')	2831.8	2750.4	2753.37(1)[d]	3.0
$2\nu_6$ (A')	2970.4	2871.4	2872.77(1)[d]	1.4
$2\nu_{14}$ (A')	3018.6	2846.7	2858.39(5)[d]	11.7
$2\nu_5$ (A')	3018.0	2898.9	2896.64(5)[d]	-2.3
ZPE = 15498.7 cm^{-1}				

a. Ref. [31] b. Ref. [38] c. Ref. [35] d. This work. e. Ref. [28] f. Ref. [32] g. Ref. [34] h. Ref. [39] i. Ref. [37] j. Ref. [43] k. Ref. [40] l. Ref. [41].

Table 2
CCSD(T)/ANO1 vibration-rotation interaction constants (α_i, in cm^{-1}) of C_2H_6 and C_2H_5D.

Mode	α_i^A ($\times 10^3$)	α_i^B ($\times 10^3$)	α_i^C ($\times 10^3$)
C_2H_6			
ν_1	14.3	0.52	
ν_2	-5.80	7.10	
ν_3	3.03	5.93	
ν_4	0.94	2.59	
ν_5	13.9	0.52	
ν_6	-6.90	6.99	
ν_7	8.65	0.60	
ν_8	11.1	-3.39	
ν_9	-8.50	1.15	
ν_{10}	8.73	0.38	
ν_{11}	10.1	-4.23	
ν_{12}	-4.37	2.59	
C_2H_5D			
ν_1	8.47	0.56	0.39
ν_2	9.50	0.77	0.28
ν_3	10.7	0.46	0.43
ν_4	11.7	0.60	1.16
ν_5	38.8	1.09	-5.68
ν_6	-3.22	-1.14	-5.34
ν_7	-4.37	5.95	6.32
ν_8	21.5	0.65	6.01
ν_9	56.5	5.11	1.92
ν_{10}	1.55	4.60	4.98
ν_{11}	3.51	-0.28	1.63
ν_{12}	3.33	0.53	0.59
ν_{13}	7.39	0.32	0.42
ν_{14}	38.9	-7.84	-0.64
ν_{15}	-9.97	0.55	-1.18
ν_{16}	-56.0	-0.30	2.14
ν_{17}	-17.7	1.80	0.63
ν_{18}	1.16	2.86	1.73

along with a few weaker modes with predicted infrared intensities of < 1 km/mol (the VPT2 anharmonic frequencies are summarized in Table 1). The predicted vibrational energies all fall within 5 cm^{-1} of the corresponding experimentally determined value for the fundamental vibrations and within 20 cm^{-1} for the combination modes [28,31–35,37–39].

The strongest rovibrational band in the CH stretch region of the present ethane gas-phase spectrum is at 2985.38(1) cm^{-1} and has E_u symmetry. The ν_7 fundamental band, the only pure E_u band predicted in this region, has been extensively studied and modelled, making it an ideal standard for the *ab initio* predictions [28,33,37,39,75–78]. It is noted by Villanueva et al. [28], this band exhibits perturbations (e.g., $^RQ_5$) as a result of either Fermi or Coriolis interactions with nearby overtone or combination states, and precise deperturbed rotational constants for the ν_7 mode were determined to be A = 2.6839943 cm^{-1} and B = 0.66311490 cm^{-1} [28]. The CCDS(T)/ANO1 VPT2 calculations predict A_7 = 2.6623 cm^{-1} and B_7 = 0.6624 cm^{-1} match to within the experimental uncertainty. In the present study, for simplicity, effective upper state spectroscopic constants were determined using the PGOPHER standard symmetric top Hamiltonian assuming no perturbative effects and fixing ζ, η_J, and η_K to those determined by Villanueva et al. [28]; consequently, this model is not as accurate. Despite the limitations, the presented simple model reproduces observed line positions to on average ±0.05 cm^{-1}, and the modelled intensities result in Einstein A coefficients consistent with the values from HITRAN [79]. The determined effective spectroscopic constants, A′ = 2.6824(1) cm^{-1} and B′ = 0.6631(1) cm^{-1}, are consistent with those previous experimental and *ab initio* values [28]. When combined with band origin and symmetry, the rotational constants confirm the assignment of the band at 2985.39(1) cm^{-1} as the ν_7 fundamental band, and suggest that the *ab initio* predictions are suitable for making vibrational assignments of newly measured C_2H_6 and C_2H_5D rovibrational bands.

3.3. Rovibrational structure of C_2H_5D

In contrast to the relatively sparse spectrum between 2050 - 3050 cm^{-1} (4.88 - 3.28 μm) of C_2H_6, the spectrum for C_2H_5D in the same region is relatively complex and congested. This is a result of the added D-atom breaking the degeneracy of some of the vibrational modes, and all eighteen fundamental vibrations being infrared active. The CCSD(T)/ANO1 VPT2 vibrational frequencies and α values for C_2H_5D are summarized in Tables 1 and 2. The predicted vibrational energies of the fundamental bands fall within 5 cm^{-1} of the corresponding experimentally determined values [40,41,43], and based on the agreement found for C_2H_6 the predicted values are able to accurately predict CH stretch

Table 3
Effective spectroscopic parameters[a] (in cm^{-1}) of the observed C_2H_6 rovibrational bands.

	Ground[b] (A_{1g})	ν_7 (E_u)	$\nu_8 + \nu_{11}$ (A_{2u})	ν_5 (A_{2u})
Origin	0.0	2985.39(1)	2953.92(2)	2895.62(1)
A	2.671	2.6824(1)	2.674(3)	2.666(2)
B	0.6630271	0.6631(1)	0.6651(3)	0.6794(2)
D_J ($\times 10^6$)	1.0312	0.91(9)	1.0312[c]	14.2(7)
D_{JK} ($\times 10^5$)	0.2660	0.21(7)	0.2660[c]	-33(1)
D_K ($\times 10^4$)	0.109	-0.23(1)	0.109[c]	6.36(8)
ζ		0.12828[c]	0.12828[c]	0.12828[c]
η_J ($\times 10^5$)		-7.82[c]	-7.82[c]	-7.82[c]
η_K ($\times 10^4$)		-7.12[c]	-7.12[c]	-7.12[c]

a. Experimental uncertainties are given in parentheses in units of the last significant digits. b. Ref. [33]. c. Ref. [28].

vibrations. Moreover, the CCSD(T)/ANO1 rotational constants determined by Eq. (2) for ν_{17} and ν_{18} of C_2H_5D are within < 0.02% the experimental values, e.g., the *ab initio* values are A_{17} = 2.3411, B_{17} = 0.6273, C_{17} = 0.6069 cm^{-1} compared to experimental values of $A_{Expt,17}$ = 2.3410517(13), $B_{Expt.17}$ = 0.62720325(29), $C_{Expt.17}$ = 0.60681418(29) cm^{-1} [41]. This suggests the CCSD(T)/ANO1 VPT2 rotational constants are sufficiently accurate that combined with vibrational energy they can be used to unambiguously assign newly measured vibrational states of C_2H_5D.

In the region probed in the current experimental spectrum ten infrared active bands are expected with an infrared intensity > 1 km/mol; five fundamental bands and five overtone **($\Delta v = 2$)** bands (see Table 1), as well as a large number of weaker vibrational transitions that should not be observable at the current experimental signal-to-noise. As seen for the normal isotopologue, the 3–4 μm region of C_2H_5D is complicated due to perturbations by overtones and combination states (with a low-frequency torsional mode (ν_{18}) at ~277 cm^{-1}) that are in Fermi or Coriolis resonance. For example, a Fermi resonance is predicted between the ν_4 and $2\nu_9$ state, which results in the infrared intensity borrowing between the two states; ν_4 to increase from about 6 to 11 km/mol and $2\nu_9$ to decrease from about 8 to 1 km/mol.

At the signal-to-noise of the present experimental spectrum only eight rovibrational bands are observed (see Fig. 3). The best fit modelled spectra based on the standard Watson non-rigid asymmetric top Hamiltonian reproduces observed line positions to ± 0.1 cm^{-1}. Some transitions are missing or blended in the modelled spectra when compared to the observed high resolution experimental spectra. The absorption modelled by the assumed dipole moment is consequently spread out over only the limited number of transitions captured in the best fit model. As a result, the modelled band intensities match the observed experimental intensities in the convoluted spectra, but at the experimental resolution individual line intensities end up being overestimated in the modelled spectra.

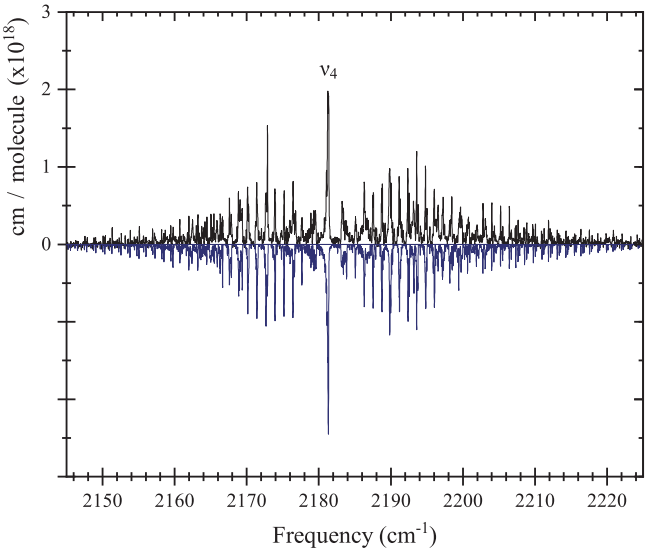

Fig. 4. C_2H_5D experimental spectrum (in black) in the CD stretch region with the ν_4 rovibrational band simulated inverted below (in blue using PGOPHER [47]).

Based on the band origins determined from the models, the eight bands are tentatively assigned as the ν_1, ν_2, ν_4, and ν_{12} fundamental bands, and the $2\nu_5$, $2\nu_6$, $2\nu_7$, and $2\nu_{14}$ overtone bands. The effective upper state rotational constants for the eight bands are determined from the best fit of the models (Table 4) and are found to be within 1% agreement of theoretical values confirming the vibrational assignments. For bands where higher order centrifugal terms could not be determined the values are fixed to the ground state values of Daly et al. [40].

In the CD stretch region of the C_2H_5D experimental spectrum only one rovibrational band is observed, at 2181.38(1) cm^{-1} with A-type and B-type transitions of an A′ - A′ vibrational transition. Combined with the determined effective rotational constants (see Table 4), this band is assigned the CD stretch (ν_4) fundamental band (see Fig. 4). In this region, no additional spectral features can be identified, e.g. the $2\nu_9$ overtone band predicted at 2239.0 cm^{-1}, suggesting that the presence of the predicted Fermi resonance between ν_4 and $2\nu_9$ that results in the significant intensity borrowing from $2\nu_9$.

Table 4
Effective spectroscopic parameters[a] (in cm^{-1}) and tentative vibrational assignments of the observed C_2H_5D rovibrational bands.

	Ground[b] (A')	ν_{12} (A")	ν_2 (A')	ν_1 (A')	$2\nu_5$ (A')	$2\nu_6$ (A')	$2\nu_{14}$ (A')	$2\nu_7$ (A')	ν_4 (A')
Origin	0.0	2975.71(1)[c]	2952.18(5)	2948.30(1)	2896.64(5)	2872.77(1)	2858.39(5)	2753.37(1)	2181.38(1)
A	2.3233871(8)	2.299(1)	2.314(2)	2.317(1)	2.311(3)	2.326(2)	2.246[d]	2.323(1)	2.319(1)
B	0.6290712(3)	0.629(2)	0.630(5)	0.628(1)	0.645[d]	0.630(5)	0.627[d]	0.620(1)	0.630(1)
C	0.6075590(3)	0.609(2)	0.602(5)	0.608(1)	0.609[d]	0.613(5)	0.619[d]	0.599(1)	0.607(1)
Δ_K ($\times 10^5$)	0.81775(14)	-5.11(57)	0.81775[e]	0.81775[e]	0.81775[e]	0.81775[e]	0.81775[e]	0.81775[e]	1.10(94)
Δ_{JK} ($\times 10^6$)	2.2144(2)	-3.4(9)	2.2144[e]	2.2144[e]	2.2144[e]	2.2144[e]	2.2144[e]	2.2144[e]	30.83(60)
Δ_J ($\times 10^6$)	0.89671(6)	2.46(51)	0.89671[e]	0.89671[e]	0.89671[e]	0.89671[e]	0.89671[e]	0.89671[e]	5.38(86)
δ_K ($\times 10^8$)	-3.373(1)	-3.373[e]	-3.373[e]	-3.373[e]	-3.373[e]	-3.373[e]	-3.373[e]	-3.373[e]	-3.373[e]
δ_J ($\times 10^9$)	2.753(6)	2.753[e]	2.753[e]	2.753[e]	2.753[e]	2.753[e]	2.753[e]	2.753[e]	2.753[e]
H_K ($\times 10^{10}$)	1.56(6)								
H_{KJ}									
H_{JK} ($\times 10^{12}$)	6.67(2)								
H_J ($\times 10^{13}$)	1.4(4)								

a. Experimental uncertainties are given in parentheses in units of the last significant digits. b. Ref. [40]. c. Band origin for $K'_a \geq 2$ subbands. For $K'_a = 0$ subband: ν_0 = 2979.14(5) cm^{-1} and $K'_a = 1$ subband: ν_0 = 2980.84(5) cm^{-1}. d. Fixed to CCSD(T)/ANO1 VPT2 values. e. Fixed to ground state values [40].

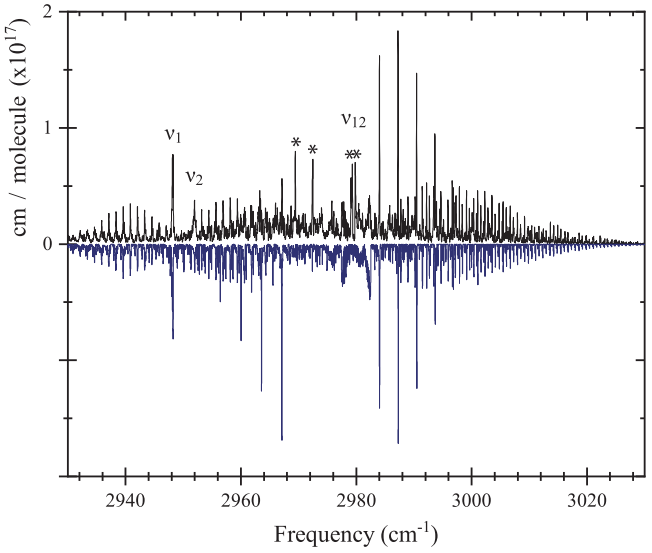

Fig. 5. C_2H_5D experimental spectrum (in black) in the CH stretch region with the summed trace of the ν_1, ν_2, and ν_{12} rovibrational bands simulated inverted below (in blue using PGOPHER [47]). Strong features that could not be assigned to a rovibrational transition are marked with asterisk (*) symbols.

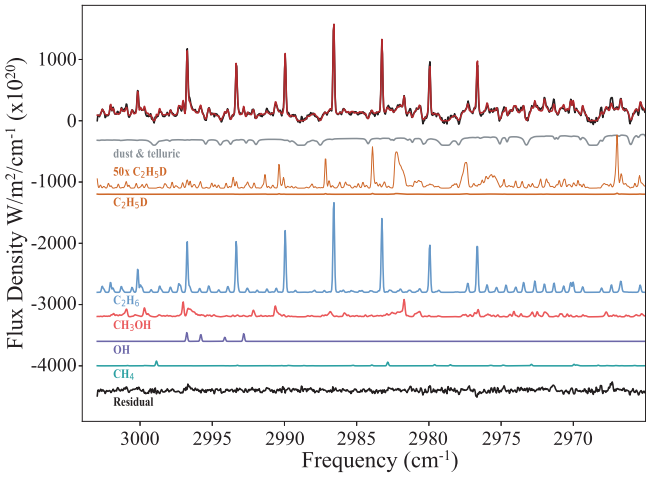

Fig. 6. Best fluorescence model fit (upper red trace) to the observed emission spectra of the comet C/2007 W1 (Boattini; upper black trace), including spectral features due to dust and telluric lines, C_2H_5D, C_2H_6, CH_3OH, OH, and CH_4 (individual simulated emission features are given in lower colored traces). The residual of the best fit is shown in black in the lowest trace. A trace of the C_2H_5D spectrum at $50\times$ the actual abundance is given to indicate the spectral morphology at the resolving power of the observations.

In the spectral forest observed in the CH stretch region, six complete rovibrational bands and one strong Q-branch are identifiable with band origins at 2975.71(1), 2952.18(5), 2948.30(1), 2896.64(5), 2872.77(1), 2858.39(5), and 2753.37(1) cm^{-1} (see Fig. 5). Additional spectral lines are observed in the experimental spectrum, including possible Q-branches marked with asterisks in Fig. 5, but no band structure is recognizable. Like the band in the CD stretch region, the rovibrational bands in the CH stretch region show a mix of A-type and B-type transitions of A′ - A′ vibrational transitions, with the exception of the band at 2975.71(1) cm^{-1}, which shows C-type transitions of a A′ - A″ vibrational transition. Based on the effective rotational constants and vibrational energies given in Table 4, the upper states are tentatively assigned as the $2\nu_7$, $2\nu_{14}$, $2\nu_6$, $2\nu_5$, ν_1, ν_2, and ν_{12} states. The strongest band in the experimental spectrum is the ν_{12} fundamental, which is the equivalent vibration to the ν_7 mode of C_2H_6 - the CH_3 asymmetric stretch vibration.

As a result of the higher state density around 3000 cm^{-1} relative to 2000 cm^{-1}, the vibrational states in this energy range experience more complex state mixing, involving both Fermi and Coriolis interactions. In the experimental spectrum evidence for state mixing is observed prominently in two of the rovibrational bands: $2\nu_5$ and ν_{12}. In order to reproduce the observed ν_{12} fundamental band structure, the $K'_a = 0$ and 1 subband origins (ν_0) are shifted relative to the $K'_a \geq 2$ subbands, giving subband origins of: $K'_a = 0$ is 2979.14(5) cm^{-1}, $K'_a = 1$ is 2980.84(5) cm^{-1}, and $K'_a \geq 2$ is 2975.71(1) cm^{-1}. A similar shifting of the K'_a subbands is observed for the $2\nu_5$ overtone band. This suggests a K'_a dependent perturbation, e.g. a Coriolis interaction. However, spectral confusion around 2900 cm^{-1} precludes accurate rotational assignment of the $2\nu_5$ overtone band, but the VPT2 predicted rotational constants sufficiently reproduce the observed Q-branch structure.

4. Modeling C_2H_5D in cometary atmospheres

Comae of comets are highly diffuse and collision between molecules are too rare to establish thermodynamic equilibrium. Instead, radiation dominates the molecule's rovibrational state population, with solar radiation "pumping" molecules into vibrationally excited states. This in turn results in subsequent fluorescent emission through radiative decay. Infrared active transitions are thus seen in emission in spectroscopic observation of comets. The strength of a solar-pumped fluorescent line is not only dependent on the molecules' abundance, but requires computation of the transition-dependent fluorescent emission rates or g factors [28]. Effectively, the rate at which a certain state is populated is determined by the absorption of Solar radiation and emission from this state is subsequently proportional to the Einstein A coefficient of the particular transition. The quantum band models for the different rovibrational transitions are used to derive fluorescent pumping and emission rates. Following the procedures described in Appendix C of Villanueva et al. [28], the state-specific fluorescent solar pumping rates, $g_{pump}(L')$, are obtained by summing over all transitions leading to state L'. The fluorescent emission of a particular transition, the g factor, is the product of the solar pumping rate and the relative strength of the Einstein A coefficient with respect to all transitions to this state.

The new rovibrational band models are applied to the emission spectra of the comet C/2007 W1 (Boattini) to look for infrared features from deuterated ethane. The comet C/2007 W1 was a dynamically new comet that had particularly favorable observing conditions, getting as close as 0.2 AU from the Earth [80,81]. The data for this study, and presented in Fig. 6 were taken on July 9, 2008, using the long-slit echelle grating spectrograph at Keck-2, NIRSPEC with the KL1 setting (see Villanueva et al. 2011 for details) [80,82]. Of the 21 comets in our NIRSPEC/Keck II spectral database, the comet C/2007 W1 is a representative comet in terms of absolute Doppler shift (km/s) and fluorescence brightness (FoM), which makes it a good candidate for determining a diagnostic upper limit for D/H in ethane.

Based on the best fit of the fluorescence model to the observed emission spectra of the comet C/2007 W1 (Boattini; see Fig. 6), the molecular production rates are determined to be (without correcting for Q-scale, nucleocentric production rates, see Villanueva et al. [28] for details): $1.461(9)\times10^{26}$ molecules/s (C_2H_6); $3.45(7)\times10^{26}$ molecules/s (CH_3OH); $1.69(31)\times10^{26}$ molecules/s (CH_4); $9.28(71)\times10^{27}$ molecules/s (OH); and $< 2.49\times10^{24}$ (3σ upper limit) molecules/s (C_2H_5D). Assuming that most deuterated

ethane is monodeuterated, and accounting for the possible deuteration positions, the upper limit D/H ratio for ethane is determined to be 2.6×10^{-3}. The determined upper limit D/H ratio is 18.2 × Vienna Standard Mean Ocean Water (VSMOW), and consistent with the values determined from other organics for other comets, e.g., D/H $< 5 \times 10^{-3}$ from methane for Comet C/2004 Q2 (Machholz) [18], and $\sim 25 \times 10^{-3}$ from HCN for comet Hale-Bopp [16,23,83]. The present fluorescence model has been tested and used to successfully measure ethane in the emission spectra of the comets C/2004 Q2 (Machholz) and C/2000 WM1 (LINEAR) through the ν_5 and ν_7 [84]. In particular, the comet C/2004 Q2 was determined to have an C_2H_6 abundance of $12.03(27) \times 10^{26}$ molecules/s based on the intensity of the ν_7 transitions, an abundance about 12 × that found for the comet C/2007 W1 using the same methods [84]. Consequently, assuming similar D/H for ethane would result in a C_2H_5D abundance of $< 2.9 \times 10^{25}$ molecules/s.

As seen in Hale-Bopp, a similar formation temperature ($\sim$30 K) can result in more deuterium enrichment in organics than in H_2O [16]. Due to the higher complexity of hydrocarbon organic molecules, and consequently the larger variation in specific molecular formation and fractionation pathways, a relatively higher D/H ratio and larger spread of values is expected relative to H_2O [23,85]. This is further compounded by the high exothermicity of deuterium incorporation into methane that results in higher D/H in molecules formed via CH_3^+, e.g., ethane or deuterated ethane, compared to H_2O at low temperatures such as those found for the midplane of proto-planetary disks (T > 10 K) [85]. Taking into account possible formation and fractionation pathways in proto-planetary disks, and following the protosolar disk chemical models by Cleeves et al. [23], the low deuteration of ethane observed for the comet C/2007 W1 suggests chemical processing of the cometary ice in the inner AU of the disk (within $\sim$70 AU of the protosun). This is further supported by the low observed abundance of CH_4, which is expected due to high conversion of CH_4 to C_2H_6 and larger hydrocarbons in the warm inner AU [86,87].

5. Conclusions

The high resolution infrared spectra of ethane (C_2H_6) and monodeuterated ethane (C_2H_5D) at 85 K are measured in the CD and CH stretch region. Two fundamental and one combination band of C_2H_6, and four fundamental and four overtone bands of C_2H_5D are observed and modelled using the standard symmetric top molecule and asymmetric top molecule Hamiltonians provided by the PGOPHER software [47]. The modelled rovibrational bands are sufficient to describe the main features of the C_2H_5D spectrum, and also permit a secure identification.

The emission spectra of the comet C/2007 W1 (Boattini) is modelled, and the resulting best fit parameters provide a new strict D/H upper limit of 18.2 VSMOW for ethane. The modelled cometary abundances suggest deuterium incorporation into ethane occurred in the inner region of our primordial proto-planetary disk.

Declaration of Competing Interest

The authors declare that they have no known competing financial interests or personal relationships that could have appeared to influence the work reported in this paper.

CRediT authorship contribution statement

Kirstin D. Doney: Formal analysis, Methodology, Data curation, Visualization, Writing - original draft. **Vincent Kofman:** Data curation, Writing - original draft. **Geronimo Villanueva:** Conceptualization, Funding acquisition, Supervision, Project administration, Writing - review & editing. **Keeyoon Sung:** Conceptualization, Funding acquisition, Investigation, Writing - review & editing, Validation.

Acknowledgements

This work was initiated in response to grant (15-EW15_2-0175) of the NASA Emerging Worlds Program, with financial support provided to Villanueva, Kofman and Sung. Part of research was performed at the Jet Propulsion Laboratory, California Institute of Technology, under contracts and cooperative agreements with the National Aeronautics and Space Administration. Doney would like to thank the NIST NRC Postdoctoral Research Associateship Program for financial support. The authors would like to thank John Stanton and James Thorpe for their help with the VPT2 calculations and Sarah Faggi for helpful discussions about cometary ethane.

References

[1] Epstein RI, Lattimer JM, Schramm DN. The origin of deuterium. Nature 1976;263:198–202. doi:10.1038/263198a0.
[2] Linsky JL, Draine BT, Moos HW, Jenkins EB, Wood BE, Oliveira C, et al. What is the total deuterium abundance in the local Galactic disk? Astrophys J 2006;647:1106–24. astro-ph/0608308. doi: 10.1086/505556.
[3] Mousis O, Gautier D, Bockelée-Morvan D, Robert F, Dubrulle B, Drouart A. Constraints on the formation of comets from D/Hratios measured in H_2O and HCN. Icarus 2000;148(2):513–25. doi:10.1006/icar.2000.6499.
[4] Altwegg K, Balsiger H, Bar-Nun A, Berthelier JJ, Bieler A, Bochsler P, et al. 67P/Churyumov-Gerasimenko, a Jupiter family comet with a high D/H ratio. Science 2015;347(6220). doi:10.1126/science.1261952.
[5] Alexander CMO, McKeegan KD, Altwegg K. Water reservoirs in small planetary bodies: meteorites, asteroids, and comets. Space Sci Rev 2018;214(1):36. doi:10.1007/s11214-018-0474-9.
[6] LellouchE., Bézard, B., Fouchet, T., Feuchtgruber, H., Encrenaz, T., de Graauw, T.. The deuterium abundance in jupiter and saturn from ISO-SWS observations. Astron Astrophys 2001;370(2):610–22. doi:10.1051/0004-6361:20010259.
[7] Pierel JDR, Nixon CA, Lellouch E, Fletcher LN, Bjoraker GL, Achterberg RK, et al. D/H ratios on saturn and jupiter from cassini cirs. Astron J 2017;154(5):178. doi:10.3847/1538-3881/aa899d.
[8] Donahue TM, Hoffman JH, Hodges RR, Watson AJ. Venus was wet: a measurement of the ratio of deuterium to hydrogen. Science 1982;216(4546):630–3. doi:10.1126/science.216.4546.630.
[9] Villanueva GL, Mumma MJ, Novak RE, Käufl HU, Hartogh P, Encrenaz T, et al. Strong water isotopic anomalies in the martian atmosphere: probing current and ancient reservoirs. Science 2015;348(6231):218–21. doi:10.1126/science.aaa3630.
[10] Tielens AGGM. The D/H ratio in molecular clouds. In: Singh PD, editor. Astrochemistry of Cosmic Phenomena. IAU Symposium, 150; 1992. p. 91.
[11] Roberts H, Fuller GA, Millar TJ, Hatchell J, Buckle JV. Molecular D/H ratios in the dense gas surrounding low-mass protostars. Planet Space Sci 2002;50:1173–8. doi:10.1016/S0032-0633(02)00079-X.
[12] Sandford SA. Interstellar processes leading to molecular deuterium enrichment and their detection. Planet Space Sci 2002;50(12):1145–54. doi:10.1016/S0032-0633(02)00075-2.
[13] Sandford SA, Bernstein MP, Dworkin JP. Assessment of the interstellar processes leading to deuterium enrichment in meteoritic organics. Meteor Planet Sci 2001;36:1117–33. doi:10.1111/j.1945-5100.2001.tb01948.x.
[14] Doney KD, Candian A, Mori T, Onaka T, Tielens AGGM. Deuterated polycyclic aromatic hydrocarbons: revisited. Astron Astrophys 2016;586:A65. doi:10.1051/0004-6361/201526809.
[15] Mumma MJ, Charnley SB. The chemical composition of comets - emerging taxonomies and natal heritage. Annu Rev Astron Astrophys 2011;49(1):471–524. doi:10.1146/annurev-astro-081309-130811.
[16] Meier R, Owen TC, Matthews HE, Jewitt DC, Bockelée-Morvan D, Biver N, et al. A determination of the HDO/H_2O ratio in comet C/1995 O1 (hale-bopp). Science 1998;279(5352):842–4. doi:10.1126/science.279.5352.842.
[17] Kawakita H, Watanabe J, Kinoshita D, Ishiguro M, Nakamura R. Saturated hydrocarbons in comet 153P/Ikeya-Zhang: ethane, methane, and monodeuteriomethane. Astrophys J 2003;590(1):573–8. doi:10.1086/374969.
[18] Bonev BP, Mumma MJ, Gibb EL, DiSanti MA, Villanueva GL, Magee-Sauer K, et al. Comet C/2004 Q2 (MACHHOLZ): parent volatiles, asearch for deuterated methane, and constraint on the CH_4spin temperature. Astrophys J 2009;699(2):1563–72. doi:10.1088/0004-637x/699/2/1563.
[19] Villanueva GL, Mumma MJ, Bonev BP, Di Santi MA, Gibb EL, Böhnhardt H, et al. A sensitive search for deuterated water in Comet 8p/Tuttle. Astrophys J Lett 2009;690(1):L5–9. doi:10.1088/0004-637X/690/1/L5.
[20] Hartogh P, Lis DC, Bockelée-Morvan D, de Val-Borro M, Biver N, Küppers M, et al. Ocean-like water in the Jupiter-family comet 103P/Hartley 2. Nature 2011;478(7368):218.
[21] BockelÉe-MorvanD., Biver, N., Swinyard, B., de Val-Borro, M., Crovisier, J., Hartogh, P., et al. Herschel measurements of the D/H and $^{16}O/^{18}O$ ratios in water in the Oort-cloud comet c/2009 P1 (Garradd). A&A 2012;544:L15. doi:10.1051/0004-6361/201219744.

[22] Gibb EL, Bonev BP, Villanueva G, DiSanti MA, Mumma MJ, Sudholt E, et al. Chemical composition of comet C/2007 N3 (Lulin): another "atypical" comet. Astrophys J 2012;750(2):102. doi:10.1088/0004-637x/750/2/102.

[23] Cleeves LI, Bergin EA, Alexander CMO, Du F, Graninger D, Öberg KI, et al. Exploring the origins of deuterium enrichments in solar nebular organics. Astrophys J 2016;819(1):13. doi:10.3847/0004-637x/819/1/13.

[24] Lis DC, Roueff E, Gerin M, Phillips TG, Coudert LH, van der Tak FFS, et al. Detection of triply deuterated ammonia in the Barnard 1 cloud. Astrophys J 2002;571:L55–8. doi:10.1086/341132.

[25] van der Tak FFS, Schilke P, Müller HSP, Lis DC, Phillips TG, Gerin M, et al. Triply deuterated ammonia in NGC 1333. Astron Astrophys 2002;388:L53–6. astro-ph/0204448. doi: 10.1051/0004-6361:20020647

[26] Parise B, Castets A, Herbst E, Caux E, Ceccarelli C, Mukhopadhyay I, et al. First detection of triply-deuterated methanol. Astron Astrophys 2004;416:159–63. astro-ph/0311038. doi: 10.1051/0004-6361:20034490.

[27] Mumma MJ, DiSanti MA, Russo ND, Fomenkova M, Magee-Sauer K, Kaminski CD, et al. Detection of abundant ethane and methane, along with carbon monoxide and water, in comet c/1996 B2 Hyakutake: evidence for interstellar origin. Science 1996;272(5266):1310–14. doi:10.1126/science.272.5266.1310.

[28] Villanueva GL, Mumma MJ, Magee-Sauer K. Ethane in planetary and cometary atmospheres: transmittance and fluorescence models of the ν_7 band at 3.3 µm. J Geophys Res 2011;116(E8). doi:10.1029/2010JE003794.

[29] Boudin N, Schutte WA, Greenberg JM. Constraints on the abundances of various molecules in interstellar ice: laboratory studies and astrophysical implications. Astron Astrophys 1998;331:749.

[30] Herzberg G.. Electronic spectra and electronic structure of polyatomic molecules. 1966.

[31] Lepard DW, Shaw DE, Welsh HL. The ν_{10} and ν_{11} raman bands of gaseous ethane. Can J Phys 1966;44(10):2353–62. doi:10.1139/p66-192.

[32] Susskind J. Torsion-vibration-rotation interaction in ethane: the bands ν_{12} + ν_4, ν_8 and ν_6. J Mol Spectrosc 1974;49(3):331–42. doi:10.1016/0022-2852(74)90015-0.

[33] Pine AS, Lafferty W. Torsional splittings and assignments of the doppler-limited spectrum of ethane in the CH stretching region. J Res Natl Bur Stand 1982;87:237–56.

[34] Henry L, Valentin A, Lafferty W, Hougen J, Devi VM, Das P, et al. Analysis of high resolution fourier transform and diode laser spectra of the ν_9 band of ethane. J Mol Spectrosc 1983;100(2):260–89. doi:10.1016/0022-2852(83)90086-3.

[35] Fernández-Sánchez JM, Valdenebro AG, Montero S. The torsional Raman spectra of C_2H_6 and C_2D_6. J Chem Phys 1989;91(6):3327–34. doi:10.1063/1.456908.

[36] Bermejo D, Santos J, Cancio P, Ferneández-Sánchez JM, Montero S. Vibrational-torsional coupling. High-resolution stimulated Raman spectrum of the ν_3 band of ethane ($^{12}C_2H_6$). J Chem Phys 1992;97(10):7055–63. doi:10.1063/1.463531.

[37] Hepp M, Herman M. Weak combination bands in the 3-µm region of ethane. J Mol Spectrosc 1999;197(1):56–63. doi:10.1006/jmsp.1999.7893.

[38] Moazzen-Ahmadi N. A combined frequency analysis of the ν_3, ν_9, $3\nu_4$ and the far-infrared bands of ethane: a reassessment of the torsional parameters for the ground vibrational state. J Mol Spectrosc 2002;214(2):144–51. doi:10.1006/jmsp.2002.8599.

[39] Fernández JM, Montero S. Torsional selection rules, Raman tensors, and cross sections for degenerate modes of C_2H_6. J Chem Phys 2003;118(6):2657–72. doi:10.1063/1.1535420.

[40] Daly AM, Drouin BJ, Groner P, Yu S, Pearson JC. Analysis of the rotational spectrum of the ground and first torsional excited states of monodeuterated ethane, CH_3CH_2D. J Mol Spectrosc 2015;307:27–32. doi:10.1016/j.jms.2014.11.002.

[41] Daly AM, Drouin BJ, Pearson JC, Sung K, Brown LR, Mantz A, et al. The ν_{17} band of C_2H_5D from 770 to 880cm^{-1}. J Mol Spectrosc 2015;316:1–10. doi:10.1016/j.jms.2015.06.006.

[42] Hirota E, Endo Y, Saito S, Yoshida K, Yamaguchi I, Machida K. Microwave spectra of deuterated ethylenes: dipole moment and r_z structure. J Mol Spectrosc 1981;89(1):223–31. doi:10.1016/0022-2852(81)90171-5.

[43] Kondo S, Saëki S. Infrared absorption intensities of ethane and propane. Spectrochim Acta Part A 1973;29(4):735–51. doi:10.1016/0584-8539(73)80103-5.

[44] Duncan JL, Kelly RA, Nivellini GD, Tullini F. The empirical general harmonic force field of ethane. J Mol Spectrosc 1983;98(1):87–110. doi:10.1016/0022-2852(83)90205-9.

[45] Sung K, Mantz AW, Smith MAH, Brown LR, Crawford TJ, Devi VM, et al. Cryogenic absorption cells operating inside a Bruker IFS-125HR: first results for $^{13}CH_4$ at 7µm. J Mol Spectrosc 2010;262(2):122–34. doi:10.1016/j.jms.2010.05.004.

[46] Mantz AW, Sung K, Brown LR, Crawford TJ, Smith MAH, Devi VM, et al. A cryogenic Herriott cell vacuum-coupled to a Bruker IFS-125HR. J Mol Spectrosc 2014;304:12–24. doi:10.1016/j.jms.2014.07.006.

[47] Western C.M.. PGOPHER version 8.0. 2014. University of Bristol Research Data Repository. 10.5523/bris.huflggvpcuc1zvliqed497r2

[48] Posey LR, Barker EF. The infra-red absorption spectrum of mono-deutero-ethane under high resolution. J Chem Phys 1949;17(2):182–7. doi:10.1063/1.1747209.

[49] Puzzarini C, Taylor PR. An *ab initio* study of the structure, torsional potential energy function, and electric properties of disilane, ethane, and their deuterated isotopomers. J Chem Phys 2005;122(5):054315. doi:10.1063/1.1830437.

[50] CFOUR. 2017. Coupled-Cluster techniques for Computational Chemistry, a quantum-chemical program package by J.F. Stanton, J. Gauss, M.E. Harding, P.G. Szalay with contributions from A.A. Auer, R.J. Bartlett, U. Benedikt, C. Berger, D.E. Bernholdt, Y.J. Bomble, L. Cheng, O. Christiansen, F. Engel, R. Faber, M. Heckert, O. Heun, C. Huber, T.-C. Jagau, D. Jonsson, J. Jusélius, K. Klein, W.J. Lauderdale, F. Lipparini, D.A. Matthews, T. Metzroth, L.A. Mück, D.P. O'Neill, D.R. Price, E. Prochnow, C. Puzzarini, K. Ruud, F. Schiffmann, W. Schwalbach, C. Simmons, S. Stopkowicz, A. Tajti, J. Vázquez, F. Wang, J.D. Watts and the integral packages MOLECULE (J. Almlöf and P.R. Taylor), PROPS (P.R. Taylor), ABACUS (T. Helgaker, H.J. Aa. Jensen, P. Jørgensen, and J. Olsen), and ECP routines by A. V. Mitin and C. van Wüllen. For the current version, see http://www.cfour.de.

[51] Raghavachari K, Trucks GW, Pople JA, Head-Gordon M. A fifth-order perturbation comparison of electron correlation theories. Chem Phys Lett 1989;157(6):479–83. doi:10.1016/S0009-2614(89)87395-6.

[52] Lee TJ, Scuseria GE. Achieving chemical accuracy with coupled-cluster theory. Quantum Mechanical Electronic Structure Calculations with Chemical Accuracy. Langhoff S, editor. Dordrecht: Kluwer Academic Publishers; 1995.

[53] Bartlett RJ. Coupled-cluster theory: an overview of recent developments. Modern Electronic Structure Theory, Part II. Yarkony DR, editor. Singapore: World Scientific; 1995.

[54] Gauss J, Stanton JF. Analytic CCSD(T) second derivatives. Chem Phys Lett 1997;276(1):70–7. doi:10.1016/S0009-2614(97)88036-0.

[55] Gauss J, Schleyer PvR. Encyclopedia of Computational Chemistry. New York: Wiley; 1998.

[56] Martin JML, Lee TJ, Taylor PR. A purely ab initio spectroscopic quality quartic force field for acetylene. J Chem Phys 1998;108(2):676–91. doi:10.1063/1.475429.

[57] Thorwirth S, Harding ME, Muders D, Gauss J. The empirical equilibrium structure of diacetylene. J Mol Spectrosc 2008;251(1–2):220–3. doi:10.1016/j.jms.2008.02.020.

[58] Simmonett AC, Schaefer III HF, Allen WD. Enthalpy of formation and anharmonic force field of diacetylene. J Chem Phys 2009;130(4):044301. doi:10.1063/1.3054917.

[59] McCaslin L, Stanton JF. Calculation of fundamental frequencies for small polyatomic molecules: a comparison between correlation consistent and atomic natural orbital basis sets. Mol Phys 2013;111(9–11):1492–6. doi:10.1080/00268976.2013.811303.

[60] Doney KD, Zhao D, Linnartz H. High-resolution infrared spectra of the ν_1 fundamental bands of mono-substituted ^{13}C propyne isotopologues. J Phys Chem A 2018;122(2):582–9. doi:10.1021/acs.jpca.7b10721.

[61] Doney KD, Zhao D, Stanton JF, Linnartz H. Theoretical investigation of infrared spectra of small polyynes. PCCP 2018;20:5501–8. doi:10.1039/C7CP06131E.

[62] Woon DE, Dunning Jr TH. Gaussian basis sets for use in correlated molecular calculations. V. Core-valence basis sets for boron through neon. J Chem Phys 1995;103(11):4572–85. doi:10.1063/1.470645.

[63] Feller D. The role of databases in support of computational chemistry calculations. J Comput Chem 1996;17(13):1571–86.

[64] Schuchardt KL, Didier BT, Elsethagen T, Sun L, Gurumoorthi V, Chase J, et al. Basis set exchange: a community database for computational sciences. J Chem Inf Model 2007;47(3):1045–52. doi:10.1021/ci600510j.

[65] Auer AA, Gauss J. Equilibrium structure and fundamental frequencies of allene. PCCP 2001;3:3001–5. doi:10.1039/B103342P.

[66] Bak KL, Gauss J, Jørgensen P, Olsen J, Helgaker T, Stanton JF. The accurate determination of molecular equilibrium structures. J Chem Phys 2001;114(15):6548–56. doi:10.1063/1.1357225.

[67] Zhang X, Maccarone AT, Nimlos MR, Kato S, Bierbaum VM, Ellison GB, et al. Unimolecular thermal fragmentation of ortho-benzyne. J Chem Phys 2007;126(4):044312. doi:10.1063/1.2409927.

[68] Simandiras ED, Rice JE, Lee TJ, Amos RD, Handy NC. On the necessity of F basis functions for bending frequencies. J Chem Phys 1988;88(5):3187–95. doi:10.1063/1.453963.

[69] Jensen F. The magnitude of intramolecular basis set superposition error. Chem Phys Lett 1996;261(6):633–6. doi:10.1016/0009-2614(96)01033-0.

[70] Almlöf J, Taylor PR. General contraction of Gaussian basis sets. I. Atomic natural orbitals for first- and second-row atoms. J Chem Phys 1987;86(7):4070–7. doi:10.1063/1.451917.

[71] Bauschlicher Jr CW, Taylor PR. Atomic natural orbital basis sets for transition metals. Theor Chim Acta 1993;86(1):13–24. doi:10.1007/BF01113513.

[72] Martin JML, Taylor PR, Lee TJ. The harmonic frequencies of benzene. A case for atomic natural orbital basis sets. Chem Phys Lett 1997;275(3):414–22. doi:10.1016/S0009-2614(97)00735-5.

[73] Vázquez J, Stanton JF. Treatment of Fermi resonance effects on transition moments in vibrational perturbation theory. Mol Phys 2007;105(1):101–9. doi:10.1080/00268970601135784.

[74] Matthews DA, Vázquez J, Stanton JF. Calculated stretching overtone levels and Darling-Dennison resonances in water: a triumph of simple theoretical approaches. Mol Phys 2007;105(19–22):2659–66. doi:10.1080/00268970701618424.

[75] Cole ARH, Cross KJ, Cugley JA, Heise HM. Infrared rotation-vibration spectra of ethane: the perpendicular band, ν_7, of C_2H_6. J Mol Spectrosc 1980;83(2):233–44. doi:10.1016/0022-2852(80)90047-8.

[76] Melen F, Herman M, Matti G, Mcnaughton D. Fourier transform jet spectrum of the $\nu_7$band of C_2H_6. J Mol Spectrosc 1993;160(2):601–3. doi:10.1006/jmsp.1993.1208.

[77] Pine AS, Stone SC. Torsional tunneling and A_1-A_2 splittings and air broadening of the $^rQ_0$ and $^pQ_3$ subbranches of the ν_7 band of ethane. J Mol Spectrosc 1996;175(1):21–30. doi:10.1006/jmsp.1996.0004.

[78] Pine AS, Rinsland CP. The role of torsional hot bands in modeling atmo-

spheric ethane. J Quant Spectrosc Radiat Transfer 1999;62(4):445–58. doi:10.1016/S0022-4073(98)00114-9.
[79] Gordon I, Rothman L, Hill C, Kochanov R, Tan Y, Bernath P, et al. The hitran2016 molecular spectroscopic database. J Quant Spectrosc Radiat Transfer 2017;203:3–69. doi:10.1016/j.jqsrt.2017.06.038. HITRAN2016 Special Issue
[80] Villanueva GL, Mumma MJ, DiSanti MA, Bonev BP, Gibb EL, Magee-Sauer K, et al. The molecular composition of comet c/2007 w1 (boattini): evidence of a peculiar outgassing and a rich chemistry. Icarus 2011;216(1):227–40. doi:10.1016/j.icarus.2011.08.024.
[81] Lippi M, Villanueva GL, Mumma MJ, Camarca MN, Faggi S, Paganini L. New insights into the chemical composition of five oort cloud comets after re-analysis of their infrared spectra. Astron J 2020;159(4):157. doi:10.3847/1538-3881/ab7206.
[82] McLean IS, Becklin EE, Bendiksen O, Brims G, Canfield J, Figer DF, et al. Design and development of NIRSPEC: a near-infrared echelle spectrograph for the Keck II telescope. In: Fowler AM, editor. Infrared Astronomical Instrumentation; vol. 3354. International Society for Optics and Photonics. SPIE; 1998. p. 566–78. doi:10.1117/12.317283.
[83] Eberhardt P, Reber M, Krankowsky D, Hodges RR. The D/H and $^{18}O^{16}O$ ratios in water from comet P/Halley.. Astron Astrophys 1995;302:301.
[84] Radeva YL, Mumma MJ, Villanueva GL, A'Hearn MF. A newly developed fluorescence model for $C_2H_6\,\nu_5$ and application to cometary spectra acquired with nirspec at keck ii. Astrophys J 2011;729(2):135. doi:10.1088/0004-637x/729/2/135.
[85] Aikawa Y, Herbst E. Deuterium fractionation in protoplanetary disks. Astrophys J 1999;526(1):314–26. doi:10.1086/307973.
[86] Gerakines PA, Schutte WA, Ehrenfreund P. Ultraviolet processing of interstellar ice analogs. I. Pure ices. Astron Astrophys 1996;312:289–305.
[87] Gerakines PA, Moore MH, Hudson RL. Energetic processing of laboratory ice analogs: UV photolysis *versus* ion bombardment. J Geophys Res 2001;106(E12):33381–5. doi:10.1029/2000JE001320.